ACCOUNTS of chemical research

pubs.acs.org/accounts Article

Viruses Masquerading as Antibodies in Biosensors: The Development of the Virus BioResistor

Apurva Bhasin, Nicholas P. Drago, Sudipta Majumdar, Emily C. Sanders, Gregory A. Weiss,* and Reginald M. Penner*

Cite This: https://dx.doi.org/10.1021/acs.accounts.0c00474 Read Online

ACCESS | Metrics & More | Article Recommendations

CONSPECTUS: The 2018 Nobel Prize in Chemistry recognized in vitro evolution, including the development by George Smith and Gregory Winter of phage display, a technology for engineering the functional capabilities of antibodies into viruses. Such bacteriophages solve inherent problems with antibodies, including their high cost, thermal lability, and propensity to aggregate. While phage display accelerated the discovery of peptide and protein motifs for recognition and binding to proteins in a variety of applications, the development of biosensors using intact phage particles was largely unexplored in the early 2000s. Virus particles, 16.5 MDa in size and assembled from thousands of proteins, could not simply be substituted for antibodies in any existing biosensor architectures.

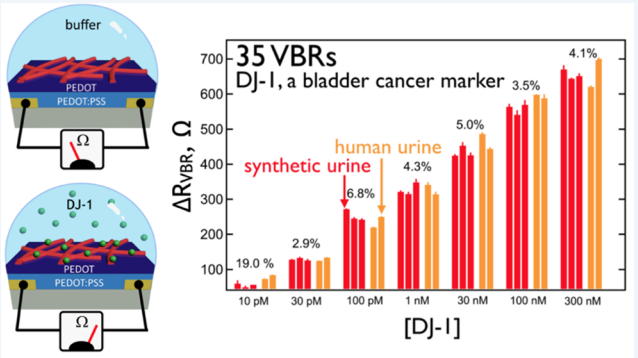

Incorporating viruses into biosensors required us to answer several questions: What process will allow the incorporation of viruses into a functional bioaffinity layer? How can the binding of a protein disease marker to a virus particle be electrically transduced to produce a signal? Will the variable salt concentration of a bodily fluid interfere with electrical transduction? A completely new biosensor architecture and a new scheme for electrical transduction of the binding of molecules to viruses were required.

This Account describes the highlights of a research program launched in 2006 that answered these questions. These efforts culminated in 2018 in the invention of a biosensor specifically designed to interface with virus particles: the *Virus BioResistor (VBR)*. The VBR is a resistor consisting of a conductive polymer matrix in which M13 virus particles are entrained. The electrical impedance of this resistor, measured across 4 orders of magnitude in frequency, simultaneously measures the concentration of a target protein and the ionic conductivity of the medium in which the resistor is immersed. Large signal amplitudes coupled with the inherent simplicity of the VBR sensor design result in high signal-to-noise ratio (S/N > 100) and excellent sensor-to-sensor reproducibility. Using this new device, we have measured the urinary bladder cancer biomarker nucleic acid deglycase (DJ-1) in urine samples. This optimized VBR is characterized by extremely low sensor-to-sensor coefficients of variation in the range of 3−7% across the DJ-1 binding curve down to a limit of quantitation of 30 pM, encompassing 4 orders of magnitude in concentration.

KEY REFERENCES

- Yang, L. M. C.; Tam, P. Y.; Murray, B. J.; McIntire, T. M.; Overstreet, C. M.; Weiss, G. A.; Penner, R. M. Virus Electrodes for Universal Biodetection. *Anal. Chem.* **2006**, *78*, 3265−3270. *Our first biosensor exploiting immobilized virus particles instead of antibodies as receptors.*[1]
- Donavan, K. C.; Arter, J. A.; Weiss, G. A.; Penner, R. M. Virus−Poly(3,4-Ethylenedioxythiophene) Biocomposite Films. *Langmuir* **2012**, *28*, 12581−12587. *The first description and characterization of the electrodeposition of virus−PEDOT composite films.*[2]
- Bhasin, A.; Ogata, A. F.; Briggs, J. S.; Tam, P. Y.; Tan, M. X.; Weiss, G. A.; Penner, R. M. The Virus Bioresistor: Wiring Virus Particles for the Direct, Label-Free Detection of Target Proteins. *Nano Lett.* **2018**, *18*, 3623−3629. *The first paper describing the Virus BioResistor (VBR).*[3]
- Bhasin, A.; Sanders, E. C.; Ziegler, J. M.; Briggs, J. S.; Drago, N. P.; Attar, A. M.; Santos, A. M.; True, M. Y.; Ogata, A. F.; Yoon, D. V.; Majumdar, S.; Wheat, A. J.; Patterson, S. V.; Weiss, G. A.; Penner, R. M. Virus Bioresistor (VBR) for Detection of Bladder Cancer Marker DJ-1 in Urine at 10 PM in One Minute. *Anal.*

Received: July 22, 2020

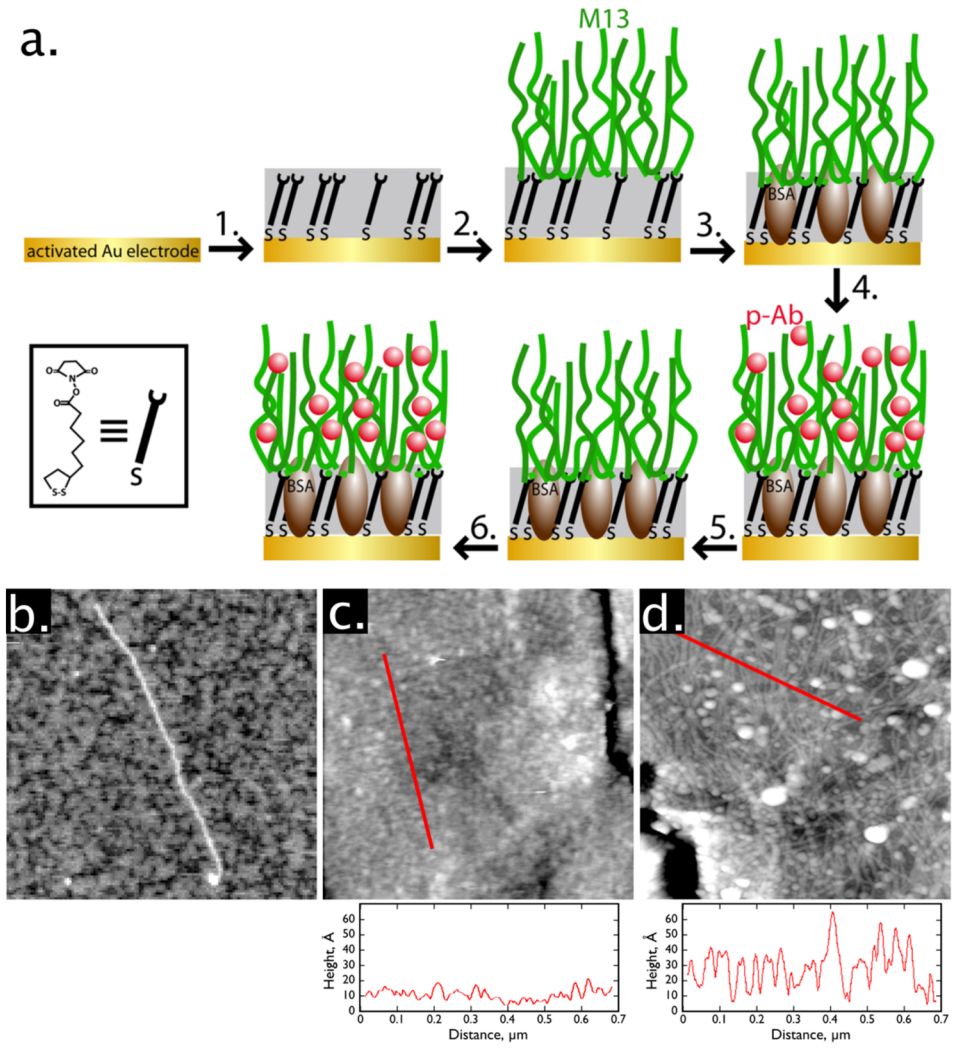

Figure 1. The covalent virus layer (CVL). (a) Stepwise assembly (steps 1−3) and functionalization (steps 4−6) of the CVL. (b−d) Noncontact mode AFM images (1 μm × 1 μm) of (b) a single M13 virion on mica, (c) a self-assembled monolayer (SAM) of *N*-hydroxysuccinimide thioctic ester (NHS-TE) on gold after exposure to BSA with no virus particles attached to the surface, and (d) a functional CVL consisting of a SAM of NHS-TE on gold that was reacted with M13 to produce covalent attachment and exposed to BSA (step 3 in (a)). Adapted from ref 13. Copyright 2008 American Chemical Society.

Chem. **2020**, *92*, 6654−6666. *The first demonstration of detection of a cancer marker in human urine, at a concentration of 10 pM, using the VBR.*[4]

1. INTRODUCTION

In 2020, the most reliable techniques used by doctors for cancer surveillance are identical to practices from 20 years ago: colonoscopy (colon cancer), mammogram (breast cancer), and Pap smear (cervical cancer). Cancer surveillance involving the analysis of blood and urine for cancer markers—so-called liquid biopsies—are not part of an annual physical examination for most Americans because biosensors and laboratory assays that facilitate rapid, reliable, and affordable analyses for cancer markers do not yet exist.

We became interested in this problem in 2005.[1] Up to this time, most biosensors designed to detect the distinctive protein "biomarkers" produced by cancers used antibodies to recognize and bind these proteins. M13, a filamentous bacteriophage that infects *Escherichia coli*, was engineered to "display" Fv antibody fragments on its surface, providing an intriguing opportunity for the development of cheaper, more robust biosensors. The basic approach for the "display" of proteins on the M13 phage surface was invented by George Smith in 1985.[5,6] Subsequently, Jim Wells and co-workers introduced key and necessary improvements that enabled Greg Winter to display an antibody, or Fv, on the phage surface.[7,8] Our laboratories exploited these seminal contributions to extend phage display into biosensing applications.

M13 viruses are an attractive alternative to antibodies in biosensors for three main reasons: (1) the cost of engineered viruses is much lower; (2) the affinity of virus particles is similar (often with dissociation constants, K_D, below 10^{-9} M); and (3) virus particles are quite robust and do not require refrigeration to maintain potency. In principle, biosensors based upon virus particles could be cheaper to manufacture and cheaper to distribute and store, especially in the resource-challenged Third World. In this Account, we trace the development over 14 years of a new biosensor, the *Virus BioResistor (VBR)*,[3,4] designed specifically for rapid (60 s) point-of-need detection of cancer markers in urine using virus receptors.

https://dx.doi.org/10.1021/acs.accounts.0c00474
Acc. Chem. Res. XXXX, XXX, XXX−XXX

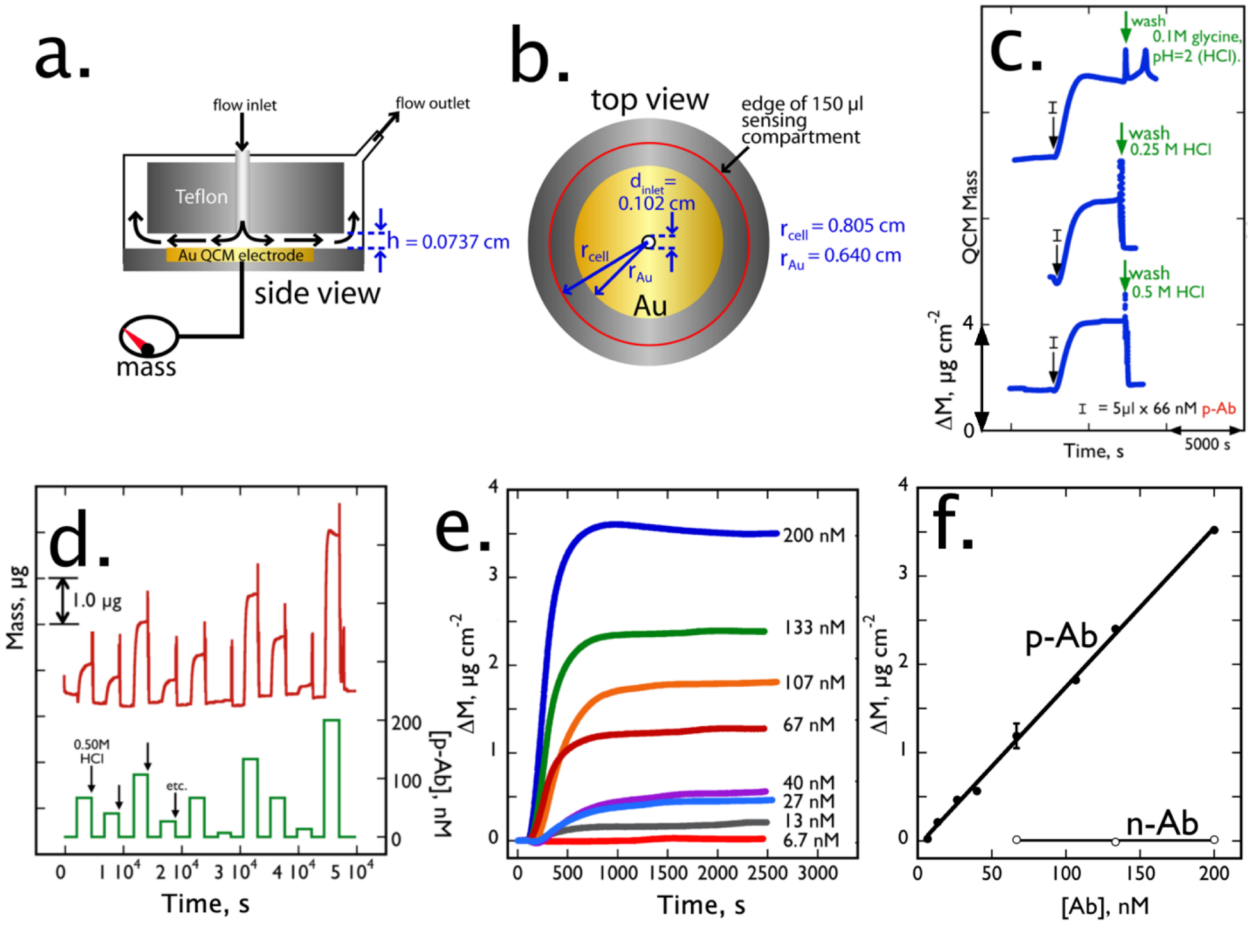

Figure 2. QCM investigations of the CVL. (a, b) Schematic diagram of the QCM and flow cell. (c) QCM evaluation of the efficacy of three wash solutions as indicated. (d) Plot of mass vs time for the exposure of a CVL to doses of P8-Ab ranging in concentration from 6.6 to 200 nM. (e) Same data as shown in (d) but normalized to the same injection time to precisely show the relative heights of these transients. (f) Plot of the maximum mass change versus P8-Ab concentration for the data shown in (d, e). The mass change was proportional to the concentration of injected P8-Ab ($R^2 = 0.997$) and yielded a sensitivity of 0.018 μg cm^{-2} nM^{-1} and a limit of detection of 6.6 nM. Adapted from ref 13. Copyright 2008 American Chemical Society.

2. VIRUS BIOSENSORS THAT RESEMBLE ANTIBODY BIOSENSORS

2.1. The Covalent Virus Layer

A generic biosensor has three components: (i) A *bioaffinity layer* equipped with receptors such as single-stranded DNA probes or antibodies to recognize and bind a target DNA or protein, respectively; (ii) a *transducer* that detects the binding of the target to the bioaffinity layer by means of a measurement of a property such as the mass of this layer or its optical or electrical response; and (iii) *electronics* that convert the raw transducer signal into a quantitative measure of the target concentration.

Bioaffinity layers for the detection of proteins have often exploited monolayers of antibodies conjugated to polymer or glass surfaces.[9] The first biosensors to exploit the Nobel Prize-winning phage-display technologies[5−8] were demonstrated in 2003 by a team at Auburn University lead by Valery Petrenko and Vitaly Vodyanoy.[10] In that work, M13 virus particles were immobilized by physisorption onto the surface of an acoustic wave sensor and used to measure the binding of β-galactosidase, a 465 kDa protein, at concentrations down to 0.60 nM.[10] These experiments provided the first proof of concept that viruses could function as receptors in biosensors. However, physisorbed virus layers,[10−12] were unstable in our measurements, compromising precision.

Li-Mei Yang, working with Juan Diaz and Phillip Tam, attempted to remedy the stability problem by preparing monolayers of M13 virus particles that were covalently bonded to a gold electrode surface (Figure 1).[13,14] Her approach was first to electrochemically roughen a gold electrode and then to expose it to thioctic *N*-hydroxysuccinimide (NHS) ester to form a thiol−Au-bonded self-assembled monolayer (SAM) and treat the SAM with a suspension of virus particles, thereby forming a covalent amide bond between free amines on the phage coat peptide and the activated carboxylate at the surface of the SAM. The final step was to plug any defects in this "covalent virus layer" (CVL) with bovine serum albumin (BSA) to minimize nonspecific adsorption (Figure 1a, step 3). The CVL is complete after step 3. Steps 4−6 in Figure 1 illustrate the reversible binding of an antibody (p-Ab) by the CVL.

Atomic force microscopy (AFM)[13,14] showed that the CVL consists of a close-packed monolayer of filamentous M13 virus particles (Figure 1b). When many M13 virus are covalently bound to a surface, the densely packed "monolayer" of the virus resembles a shag carpet (Figure 1a). The resulting CVL retains significant free volume, as evidenced by the fact that each phage particle is capable of binding 140 antibodies to the P8 major coat peptide (P8-Ab, 2700 copies/M13 virus) on average.[13] In the vacuum of a scanning electron microscope, the water and ions

https://dx.doi.org/10.1021/acs.accounts.0c00474
Acc. Chem. Res. XXXX, XXX, XXX−XXX

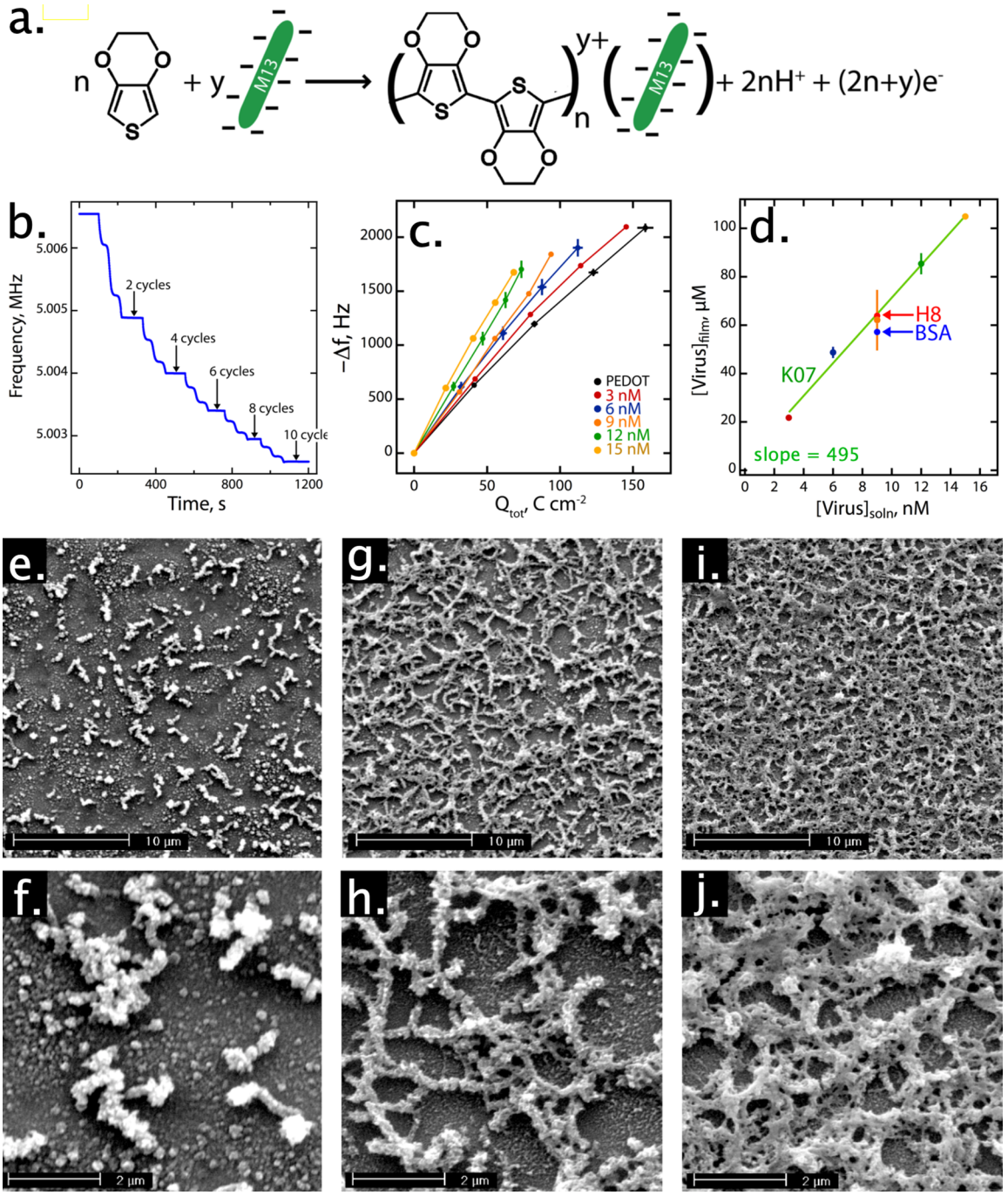

Figure 3. Electrodeposition of a virus−PEDOT bioaffinity layer. (a) Virus−PEDOT electrodeposition reaction. (b) QCM analysis of virus−PEDOT electrodeposition, with increased mass loading shown as a decrease in frequency. (c) Frequency change vs deposition charge, Q_{tot}, for QCM measurements. (d) Calibration curve showing the linear correlation of the virus concentration within the PEDOT film (vertical axis) vs the concentration of virus in solution. (e−j) Topography of virus−PEDOT films imaged by scanning electron microscopy. Films were prepared from solutions containing virus particles at three concentrations: (e, f) $[virus]_{soln}$ = 3 nM; (g, h) $[virus]_{soln}$ = 9 nM; (i, j) $[virus]_{soln}$ = 15 nM. Adapted from ref 2. Copyright 2012 American Chemical Society.

supporting the "shag carpet" are removed, and filamentous virus particles collapsed onto the surface can be clearly seen (Figure 1d).

2.2. Mass-Based Signal Transduction of the CVL

The properties of the CVL for biosensing were first explored in 2008. Both mass-based biosensing,[13] conducted by depositing the CVL on a gold quartz-crystal microbalance (QCM) transducer, and electrochemical-based sensing[14] were evaluated. In these experiments, the response of a CVL-modified gold surface to P8-Ab was studied.[13,14]

To measure the mass responses of a CVL during exposure to P8-Ab, the QCM crystal was mounted in a Teflon flow cell that provided for the radially symmetric delivery of solution to the circular QCM electrode surface (Figure 2a,b).[13] The increase in mass observed upon P8-Ab exposure (~3 $\mu g/cm^2$) could be reversed by washing briefly with aqueous acid (Figure 2c), enabling mass versus P8 antibody concentration, [P8-Ab], data

https://dx.doi.org/10.1021/acs.accounts.0c00474
Acc. Chem. Res. XXXX, XXX, XXX−XXX

to be acquired over a wide range of [P8-Ab] for a single CVL (Figure 2d–f). These data were linear from 6.6 to 200 nM P8-Ab.[13] A nonbinding antibody (n-Ab) control showed negligible nonspecific signal over this concentration range, establishing the limit of detection (LOD) for P8-Ab as 20 nM. This demonstrated that virus particles within the CVL were available for rapid binding of the antibody, suggesting that the CVL could function as a bioaffinity layer within a biosensor. Importantly, P8-Ab binding, while reversible, exhibited a very low off-rate of $<10^{-5}$ s^{-1}, indicating that reuse of the CVL would be a practical impossibility.[13] The next question was whether the binding of a target antibody could be detected using the electrochemical response of these virus-modified electrodes instead of a QCM.

2.3. Electrochemical Signal Transduction of the CVL

In addition to mass-based transduction using the QCM,[13] the electrochemical response of the CVL to P8-Ab and n-Ab were investigated using electrochemical impedance spectroscopy (EIS).[14] A goal in these experiments was to carry out *direct detection* of antibody binding to the CVL. "Direct" in this context meant that a redox couple such as $Fe(CN)_6^{4-/3-}$ was not added to the testing solution as in the "indirect" approach, in which blocking of the Faradaic electron transfer signals protein binding to an electrode surface.[15−20] Direct EIS measurements, in contrast, probed changes to the non-Faradaic impedance of the CVL-modified gold electrode caused by antibody binding to the surface.

A conclusion of these experiments was that the highest signal-to-noise ratio (S/N ≈ 20) and best selectivity for P8-Ab binding to the CVL-modified electrode occurred at high frequencies in the range of 4−140 kHz. This was surprising because the shift in the real component of the impedance signal, ΔZre, was the smallest in this frequency range, with ΔZre < 10 Ω at all P8-Ab concentrations.[14]. Selectivity for P8-Ab versus n-Ab was completely lost at lower frequencies, where ΔZ_{re} signals as large as 1 kΩ were observed. In contrast, prior work on EIS-detected indirect biosensors had emphasized the detection of target proteins at low frequencies, below 5 Hz in most cases. Z_{re} is increased by binding of P8-Ab to the CVL because the bound, insulating P8-Ab molecules displace ionically conductive electrolyte from the free volume within the CVL layer.[14] The LOD for P8-Ab in these experiments, limited by the low ΔZ_{re} signal amplitude, was 20 nM.[14]

The conclusion from these experiments was that this CVL did not afford enough sensitivity to enable the detection of proteins at subnanomolar concentrations, as required for cancer screening. A fundamentally new method for preparing a virus-based bioaffinity layer was needed.

3. VIRUS−PEDOT BIOAFFINITY LAYERS

3.1. Electrodeposition of a Virus−PEDOT Composite Film

Inspiration for a new type of virus-based bioaffinity layer arrived from an unexpected direction. In the 2010 time frame, the Penner group had been investigating the thermoelectric properties of nanowires composed of the electronically conductive organic polymer poly(3,4-ethylenedioxythiophene) (PEDOT).[21] These PEDOT nanowires were prepared using lithographically patterned nanowire electrodeposition (LPNE).[22,23]

Could PEDOT act as a host for M13 virus particles? This idea was interesting for two reasons: First, the electronic conductivity of PEDOT provided a means by which the biosensor signal from M13 particles could be directly transmitted to an external circuit. Second, PEDOT is positively charged as synthesized, with one positive charge for each four or five EDOT residues. During electropolymerization (Figure 3a), EDOT is oxidized to a cation radical, and radical coupling occurs near the electrode surface until the resulting oligomers lose solubility and, with anions from the solution to balance the positive charge, precipitate onto the electrode. M13 virus particles have a net negative charge near 6000 as a consequence of three ionizable moieties (Glu2, Asp4, and Asp5) on the 2700-copy P8 major coat protein near its exposed N-terminus.[24] Our hypothesis was that the polymerization of positively charged PEDOT in the presence of negatively charged M13 would electrostatically promote the incorporation of M13 particles within the polymer matrix.

To test this hypothesis, virus−PEDOT biocomposite films were prepared by electropolymerization of EDOT in aqueous electrolytes containing just 12 mM $LiClO_4$ and nanomolar concentrations of M13 virus particles.[2] In these experiments, it was observed that as the virus concentration was increased from 3 to 15 nM the EDOT electropolymerization current peak was depressed relative to that of the virus-free control.[2] This observation suggested that the virus particles either interfered with, or participated in, EDOT polymerization. QCM gravimetry (Figure 3b) showed that the mass of the resulting films was augmented when virus particles were present in the EDOT polymerization solution. The excess mass relative to pure PEDOT films (Figure 3c) was attributed to the incorporation of virus particles into the growing PEDOT film.[2] This observation directly demonstrated that virus particles could be incorporated into these electrodeposited PEDOT films as predicted by the reaction shown in Figure 3a.

How efficient is the virus incorporation into these films during electropolymerization? The QCM data in Figure 3c provided the answer: The difference in mass (the vertical axis) at a particular deposition charge Q_{tot} could be attributed to virus incorporated into the virus−PEDOT composite film. This analysis showed that concentration of M13 in the virus−PEDOT film prepared by electrodeposition was directly proportional to the M13 concentration in the polymerization solution (Figure 3d), and the slope of this line was an astonishing ∼500. These experiments demonstrated that the reaction shown in Figure 3a provided for highly efficient incorporation of virus into a growing PEDOT film. Scanning electron microscopy (SEM) images of electrodeposited virus−PEDOT composite films showed a striking transformation as virus was incorporated into the plating solution (Figure 3e−j). In these images, bundles of virus particles are seen protruding from the surface of the virus−PEDOT films, and as expected, the density of these virus particles is correlated with the concentration of virus in the deposition solution.[2]

3.2. Biosensing with Virus−PEDOT Nanowires

What would be the best way to exploit this new virus−PEDOT material in a biosensor? Our initial answer to this question was to prepare arrays of nanowires composed of virus−PEDOT.[25,26] These were prepared using LPNE[22,23,27] in conjunction with the same electrodeposition protocol employed for virus−PEDOT films described above.[2] The resulting virus−PEDOT nanowires, deposited onto glass surfaces, were linear, millimeters in length, ∼300 nm in width, and 60 nm in height. SEM, AFM, and fluorescence microscopy confirmed the incorporation of M13 into the conducting PEDOT nanowire arrays, and further fluorescence studies also demonstrated that the viruses remained intact and fully functional for binding to analytes.[25,26]

https://dx.doi.org/10.1021/acs.accounts.0c00474
Acc. Chem. Res. XXXX, XXX, XXX−XXX

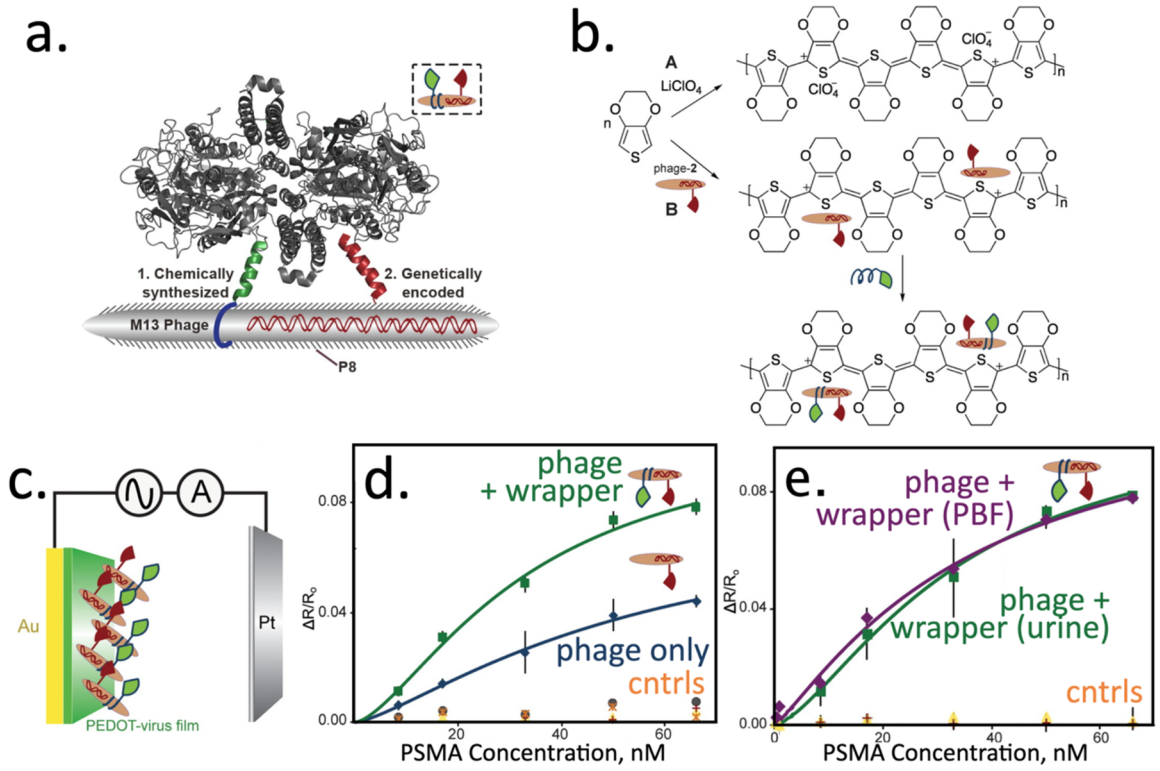

Figure 4. PSMA detection in synthetic urine using synergistic dual-ligand phage. (a) Schematic diagram of bidentate binding to PSMA by KCS-1 (green) and genetically encoded peptide (red). Simultaneous binding by these two ligands provides a higher apparent affinity for PSMA. (b) Polymerization reactions of EDOT in the presence of (top) $LiClO_4$ or (center) PSMA-binding phage and (bottom) PSMA-binding phage and exposure to the wrapper KCS-1 (green). (c) Schematic diagram of the biosensing experiment. (d) $\Delta R/R_0$ of the film increases with the PSMA concentration. (e) Comparison of PSMA detection in synthetic urine (green) with detection in PBS buffer (purple). Adapted from ref 31. Copyright 2013 American Chemical Society.

Biosensing experiments were conducted by measuring the DC resistance of a virus−PEDOT nanowire array, rather than the frequency-dependent impedance of these arrays[25,26] as in previous studies, and P8-Ab and the n-Ab control were compared. A P8-Ab concentration-dependent increase in resistance was observed, culminating in a 40% increase in response to exposure to 99 nM buffered P8-Ab solutions. An LOD for P8-Ab of 20 nM was established for these nanowire arrays. n-Ab showed no measurable signal.[25]

Arrays of virus−PEDOT nanowires were also employed for the detection of prostate-specific membrane antigen (PSMA), a promising urine-borne cancer marker for prostate cancer.[28,29] PSMA is a 750 residue, 100 kDa glycoprotein that is overexpressed as a homodimer on the surface of prostate cancer cells.[28,29] These studies exploited virus particles engineered to display the PSMA-binding epitope PSMA-3 (amino acid sequence SECVEVFQNSCDW). In spite of this change to the virus, the virus−PEDOT electrodeposition was unaffected because this process was completely modular with respect to the phage incorporation. In spite of the smaller size of PSMA relative to antibodies (100 vs 155 kDa), similar detection metrics were achieved in this study, which culminated in a PSMA LOD of 66 nM in high-salt (~160 mM) PBS buffer solutions and a linear response up to 150 nM PSMA.

The disappointing conclusion of these two studies[25,26] was that arrays of virus−PEDOT nanowires performed approximately as well as the EIS-transduced CVL-modified gold electrodes. A more direct comparison of virus−PEDOT with the CVL was needed in experiments that exploited conventional electrodes and EIS, and this was our next step.

3.3. Electrochemical Signal Transduction for Virus−PEDOT films

Compared with virus−PEDOT nanowires, a simpler approach was to coat a virus−PEDOT film onto a gold electrode. The response of such electrodes was studied using EIS for the detection of PSMA[30,31] and, separately, P8-Ab.[32] P8-Ab detection at virus−PEDOT electrodes showed a much higher S/N, ranging from 17 to 30, at high frequencies in the 100 Hz−10 kHz range. At 1 kHz, a LOD for P8-Ab of 6 nM was achieved, and quantitation of P8-Ab up to 65 nM was possible. This represented a 65% reduction in LOD for P8-Ab compared with the identical experiment conducted using CVL-modified gold electrodes.

An even better result was obtained for the detection of PSMA using a new paradigm: synergistic dual ligand phage.[30,31] The hypothesis tested in that work was that two peptide binders would be better than one. In other words, the sensitivity to PSMA could be improved by incorporating a *second* peptide binder for PSMA (called KCS-1) onto an engineered phage (phage-2) that already displayed a peptide binder for the protein (Figure 4a). This was accomplished by conjugating a positively charged oligolysine tether to the polypeptide and then permitting it to self-assemble by electrostatic attraction onto the negatively charged phage after electrodeposition of the virus−PEDOT bioaffinity layer (Figure 4b).[30,31] The addition of the second ligand, KCS-1, significantly increased the affinity of the virus for PSMA in ELISA measurements (data not shown) and for electrochemical measurements (Figure 4d). This enhanced sensitivity afforded a PSMA LOD of 100 pM in

https://dx.doi.org/10.1021/acs.accounts.0c00474
Acc. Chem. Res. XXXX, XXX, XXX−XXX

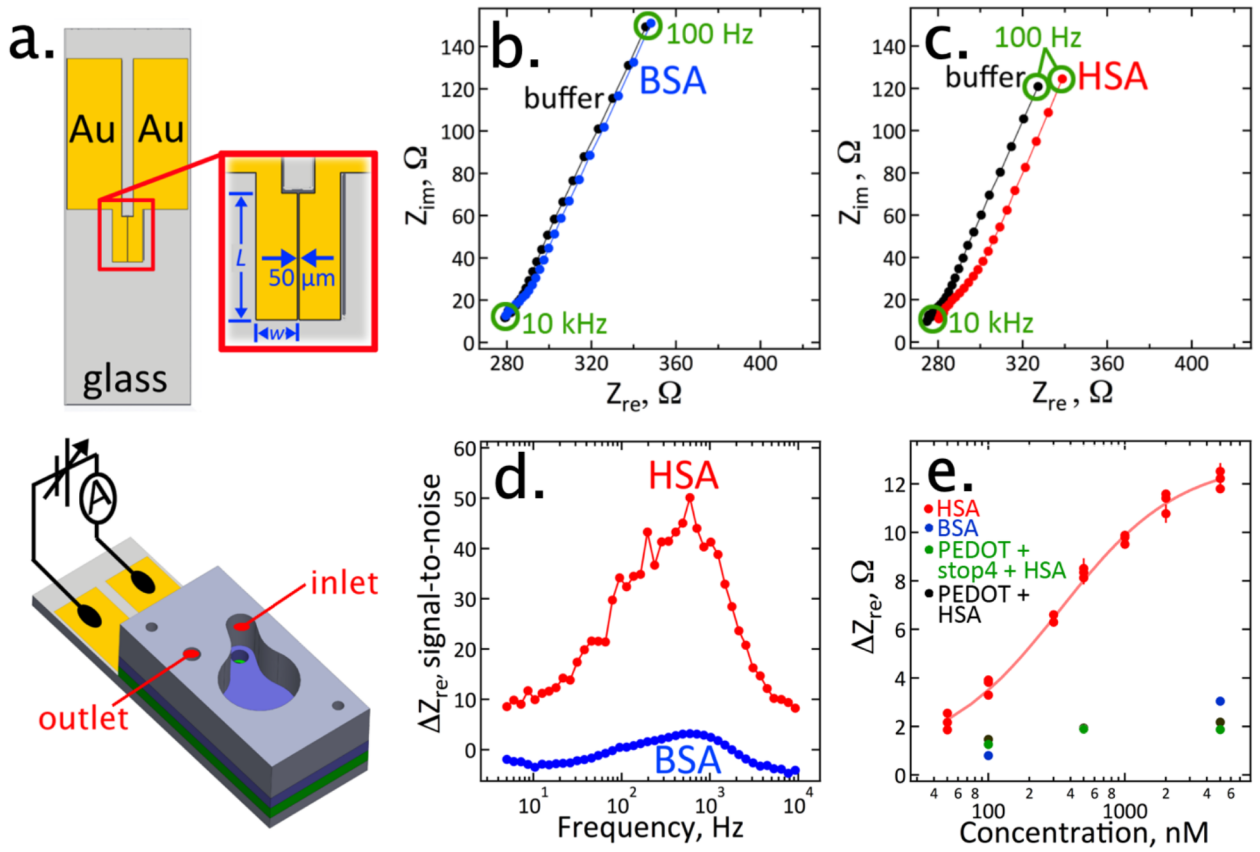

Figure 5. Two-sided biosensor: a monolithic biosensor for human serum albumin (HSA). (a) Engineering diagram of the two-electrode virus–PEDOT biosensor. (b, c) Nyquist plots (Z_{im} vs Z_{re}) for a control protein (BSA) and HSA. (d) Signal-to-noise ratio vs frequency plot for HSA and BSA. (e) ΔR_{re} vs HSA concentration calibration curve. Controls for BSA and off-virus binding are also shown. Adapted from ref 34. Copyright 2016 American Chemical Society.

buffer and in synthetic urine solutions (Figure 4e) for these dual ligand systems.

4. THE VIRUS BIORESISTOR

4.1. The two-sided virus–PEDOT biosensor

All of the virus-based biosensors investigated in our laboratories up to 2015 were laboratory experiments[1,4,13,14,25,26,30,32,33] in the sense that the electrochemical measurements were conducted using three-electrode cells incorporating separate reference, counter, and working (sensor) electrodes. A portable, miniaturizable, and commercializable electrochemical sensor architecture—in which the necessary electrodes were incorporated into a single monolithic sensor body—had not been demonstrated.

This advance occurred in 2016 with the demonstration by Alana Ogata, Ming Tan, and others that two virus–PEDOT-modified gold electrodes without reference or counter electrodes (Figure 5a) could function as a biosensor for human serum albumin (HSA).[34] Prior work on PSMA[31,33] had demonstrated that the signal generated by a virus–PEDOT-modified gold electrode was concentrated in the resistive component of the impedance, Z_{re}, instead of the capacitive component, Z_{im}. The hypothesis explored in the 2017 "two-sided" sensor architecture (Figure 5b) was that arranging *two* virus–PEDOT bioaffinity layers electrically in series would double the impedance signal produced by the biosensor.[34]

In spite of its simplicity, the two-sided virus–PEDOT biosensor reliably distinguished HSA from BSA—proteins of identical size with 76% sequence homology. This demonstrated that the inherent selectivity of the engineered virus could be recovered with this device (Figure 5b,c). At an optimized detection frequency of 340 Hz (Figure 5d), the two-sided sensor produced a prompt increase in Z_{re} within 5 s and a stable Z_{re} signal within 15 min. HSA concentrations in the range from 100 nM to 5 μM were detectable (Figure 5e). These single-use biosensors demonstrated excellent sensor-to-sensor reproducibility characterized by a coefficient of variation of 2–8% across the entire concentration range.[34] Two-sided virus–PEDOT sensors in synthetic urine demonstrated a concentration-dependent response to HSA similar to PBS buffer.

This performance provided reason for optimism, but the two-sided virus–PEDOT biosensor had two serious deficiencies. First, its 100 nM LOD for HSA was insufficient to measure cancer markers in urine at subnanomolar concentrations. The two-sided sensor simply did not produce enough signal—a *maximum* of signal of 12 Ω against a 100–200 Ω background (Figure 5e).[34] Second, the two-sided biosensor required that current be carried through the test solution between the two electrodes, thus convoluting the resistance change due to binding of the target protein with the resistance of the solution. Since urine and other bodily fluids have highly variable ionic conductivities, this imposed a barrier to the clinical use of this biosensor. In order to provide reliable results for highly variable single patient samples, a biosensor architecture that decoupled

https://dx.doi.org/10.1021/acs.accounts.0c00474
Acc. Chem. Res. XXXX, XXX, XXX–XXX

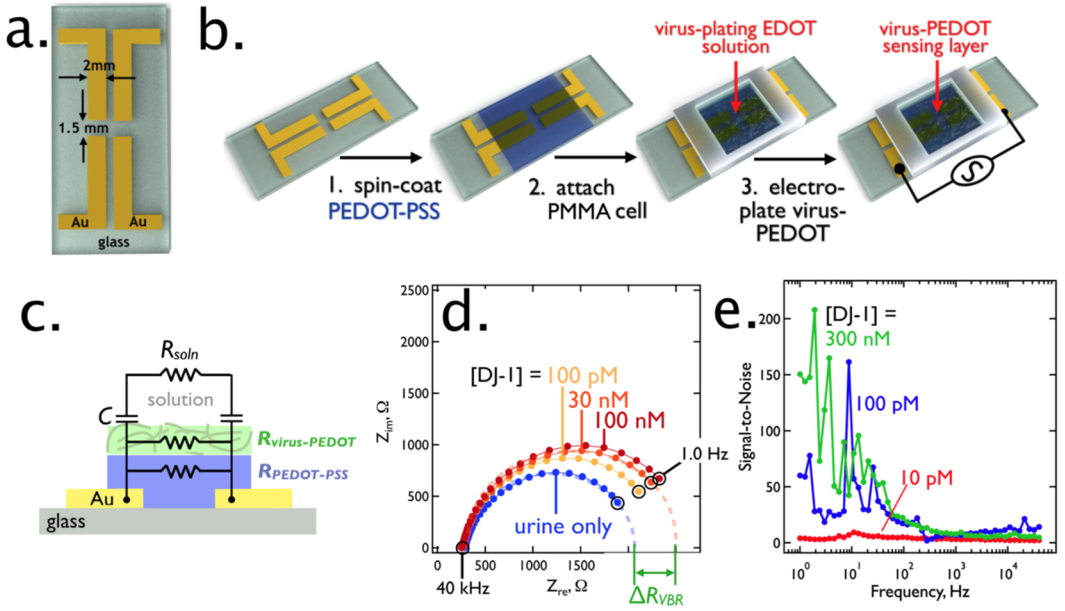

Figure 6. The Virus BioResistor. (a) The VBR is constructed on a 10 mm glass chip with patterned gold electrodes. (b) Three processing steps provide for the deposition of a PEDOT−PSS layer by spin-coating from solution (step 1), the attachment of a PMMA cell (step 2), and the electrodeposition of a virus−PEDOT layer (step 3). (c) The electrical response of the VBR is modeled by three parallel resistors and a solution/channel capacitance. (d) This circuit produces a semicircular Nyquist plot for which the high-frequency impedance (40 kHz) approximates the solution resistance ($Z_{re} \approx R_{soln}$) and the low-frequency impedance is dominated by the parallel resistance imposed by the two film resistors, $Z_{re} \approx Z_{VBR}$. Z_{VBR} increases with the concentration of target protein present in the solution phase. (e) The VBR circuit maximizes the signal-to-noise ratio at low frequencies, and S/N can exceed 100 at high protein concentrations. Adapted from ref 4. Copyright 2020 American Chemical Society.

target binding from ionic conduction was required. In spite of these two issues, the two-sided virus−PEDOT biosensor was the progenitor of the VBR.

4.2. The Virus BioResistor

Alana Ogata and Apurva Bhasin collaborated to invent the VBR in 2017 and, since then, to fully realize its capabilities.[3,4] The extension of the two-sided biosensor to the VBR is almost trivial: The virus−PEDOT bioaffinity layer was extended across the gap between the two gold electrodes. Since the virus−PEDOT layer is electrodeposited, this modification required that a conductor be deposited across this gap first. A spin-coated PEDOT layer was used for this purpose, and the virus−PEDOT layer was electrodeposited on top of it (Figure 6a,b).[3,4] We refer to this two-layer construct connecting the gold electrodes as the VBR "channel". This elaboration of the two-sided biosensor dramatically alters its properties.

When the two gold electrodes are directly connected via the channel, an internal circuit is generated for the VBR (Figure 6c) in which the resistance of the channel is arranged in parallel with the series capacitance and the resistance of the solution. This circuit produces a distinctive semicircular Nyquist plot (Z_{im} vs Z_{re} as a function of frequency) that can be modeled with two equations:[3,4]

$$-Z_{im} = \frac{\omega C_{vbr} {R_{VBR}}^2}{1 + \omega^2 {C_{vbr}}^2 (R_{sol} + R_{VBR})^2}$$

$$Z_{re} = \frac{R_{VBR}[1 + \omega^2 {C_{vbr}}^2 R_{sol}(R_{sol} + R_{VBR})]}{1 + \omega^2 {C_{vbr}}^2 (R_{sol} + R_{VBR})^2}$$

In contrast, the Nyquist plot for a two-sided biosensor produces a linear plot (Figure 5c). The response of three VBRs to the protein DJ-1, a 20 kDa bladder cancer (BC) biomarker,[35,36] shows an increase in the diameter for the semicircle (Figure 6d). This increase in diameter is produced by a shift in the low-frequency Z_{re} to higher values, while the high-frequency edge of the semicircle is unchanged. This shift in the low-frequency Z_{re} is correlated with the concentration of the target protein. One consequence of this circuit, shown in the signal-to-noise ratio versus frequency plot (Figure 6e), is that the S/N is maximized at low frequency (~1 Hz) and is negligible above 100 Hz. The high-frequency edge of the semicircle measures the solution resistance, R_{soln}. We have demonstrated[3] that these two resistors, R_{VBR} and R_{soln}, are orthogonal, allowing the value of R_{VBR} to be accurately measured independent of the value of R_{soln}. This means that the ionic resistance of the test solution does not interfere with accurate measurement of the concentration of the target protein—a critically important capability for clinical measurements.

The potential of the VBR for the detection of BC in urine is supported by the data in Figure 7.[4] Here a calibration curve for the detection of DJ-1 in both synthetic and human urine is shown (Figure 7a,b), comprising data acquired from 35 individual VBRs. These data demonstrate a lower LOD of 10 pM for DJ-1 as well as a sensor-to-sensor coefficient of variation of <7% across the DJ-1 binding curve, spanning 4 orders of magnitude, down to 30 pM.[4] The selectivity for DJ-1 (Figure 7c) was also excellent and was achieved without the use of any blocking agent (e.g., casein or BSA).[4] The signals plotted in Figure 7a,b were all measured after a brief 1 min exposure to DJ-1-spiked urine (Figure 7d).[4] However, a useful benchmark, the concentrations of DJ-1 in the urine of healthy and BC-positive patients, has not yet been established.[35,36]

The mechanism by which the VBR operates remains under investigation, but a working hypothesis is summarized by Figure 7e,f.[4] Evidence suggests that affinity-driven diffusion of the

https://dx.doi.org/10.1021/acs.accounts.0c00474
Acc. Chem. Res. XXXX, XXX, XXX−XXX

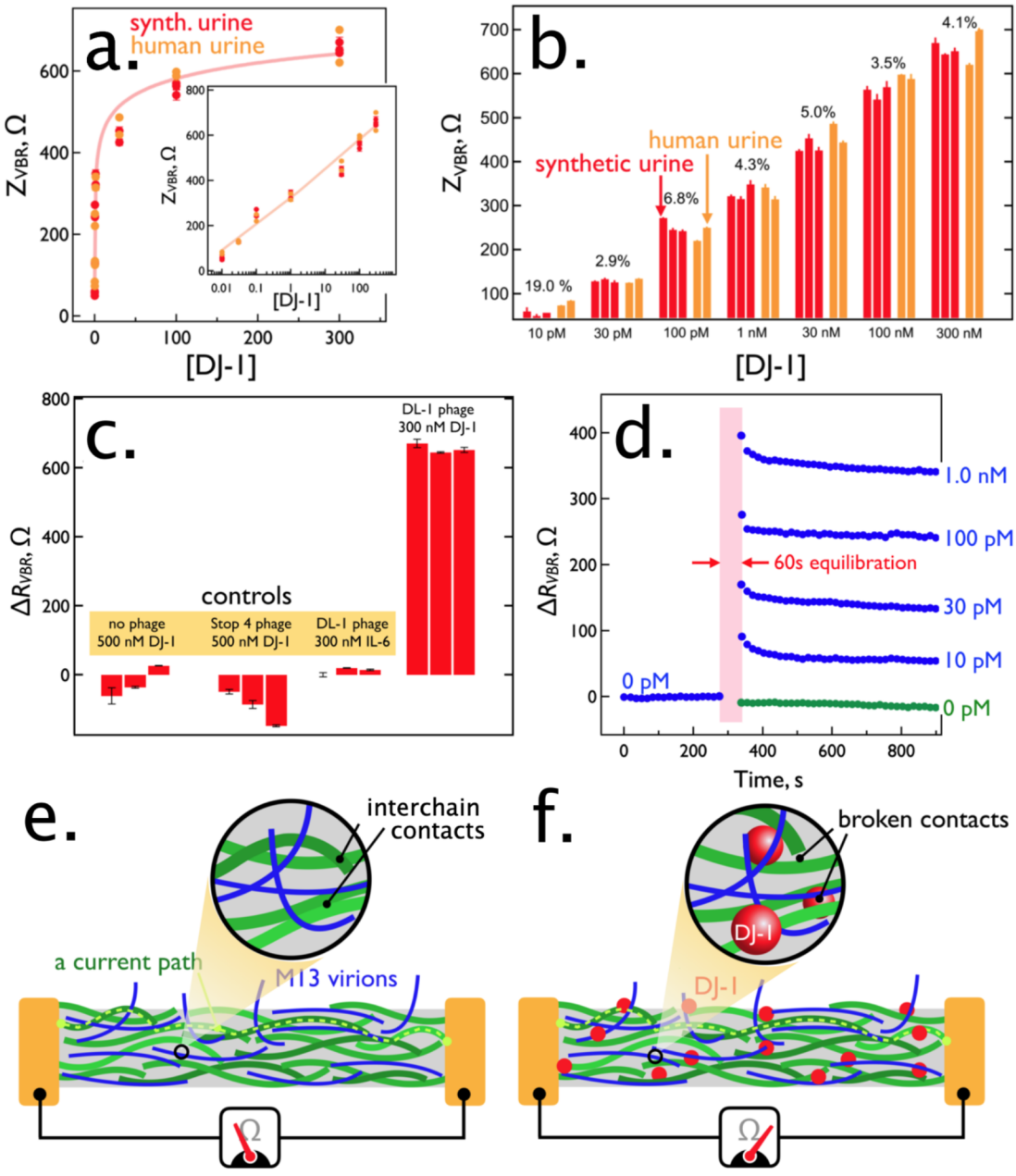

Figure 7. Rapid quantitation of DJ-1 in urine. (a, b) Correlation of the VBR signal against DJ-1 concentration in urine and synthetic urine. (c) Comparison of the DJ-1 signal at 300 nM with three controls. (d) VBR signal vs time for the exposure of five VBRs to aliquots of DJ-1 in synthetic urine. (e, f) Proposed mechanism for VBR signal transduction. Adapted from ref 4. Copyright 2020 American Chemical Society.

target protein into the virus−PEDOT layer produces an increase in its low-frequency impedance. This impedance increase may be caused by disruption of the interchain electrical contacts between PEDOT chains in this material. Further experimentation, now underway, will be required to either refute or confirm this hypothesis.[4]

4.3. Biosensor Architectures Related to the VBR

How do the VBR architecture and capabilities compare with those of other biosensors? The closest relative of the VBR is the organic electrochemical transistor (OECT).[37−39] OECTs generally have a reference electrode, in addition to source and drain electrodes, and a semiconducting polymer film channel, similar to the VBR. The device is immersed in an electrolyte solution, the source and drain are bridged by the polymer, and the reference electrode is placed in the same electrolyte solution. Biasing one of the electrodes at a set potential changes the doping level of the polymer, inducing a large conductivity change. At the same time, the potential at another electrode is swept, and the current at the third electrode is measured. This allows small changes in the doping level of the film to be measured with great accuracy.[37] By conjugation of a biorecognition element to the polymer film, low LODs (1 nM) and high specificity have been achieved for label-free detection of proteins.[40]

While OECTs can achieve detection of many analytes, these devices have limitations when it comes to clinical biomolecular sensing. High-ionic-strength solutions cause Debye screening and prevent low LODs.[41] The doping level of the polymer is

https://dx.doi.org/10.1021/acs.accounts.0c00474
Acc. Chem. Res. XXXX, XXX, XXX−XXX

dependent on the ions in the solution, which can cause issues when ion detection is not desired.[39]

5. SUMMARY AND OUTLOOK

The VBR is noteworthy for its extreme simplicity, for its use of virus particles in place of antibodies as receptors, and because its performance for the detection of some cancer markers directly on bodily fluids can be adequate for the early detection of cancer. The 14 year story of its development, recounted here, includes both dead ends (two-sided biosensors) and near failures (nanowires). That it now exists is a testament to the power of perseverance in science.

A future goal is to create arrays of VBRs in which each VBR element contains a different M13 virus particle capable of detecting a different cancer or disease marker. Such a proteomic panel might provide a multidimensional picture containing information on disease progression and tumor grade.

AUTHOR INFORMATION

Corresponding Authors

Gregory A. Weiss − *Department of Chemistry, Department of Pharmaceutical Sciences, and Department of Molecular Biology and Biochemistry, University of California, Irvine, Irvine, California 92697, United States;* orcid.org/0000-0003-0296-9846; Email: gweiss@uci.edu

Reginald M. Penner − *Department of Chemistry, University of California, Irvine, Irvine, California 92697, United States;* orcid.org/0000-0003-2831-3028; Email: rmpenner@uci.edu

Authors

Apurva Bhasin − *Department of Chemistry, University of California, Irvine, Irvine, California 92697, United States*

Nicholas P. Drago − *Department of Chemistry, University of California, Irvine, Irvine, California 92697, United States*

Sudipta Majumdar − *Department of Chemistry, University of California, Irvine, Irvine, California 92697, United States*

Emily C. Sanders − *Department of Chemistry, University of California, Irvine, Irvine, California 92697, United States;* orcid.org/0000-0003-1043-5772

Complete contact information is available at: https://pubs.acs.org/10.1021/acs.accounts.0c00474

Notes

The authors declare the following competing financial interest(s): The authors are cofounders of PhageTech Inc., a company that is commercializing some of the technologies discussed in this Account.

Biographies

Apurva Bhasin was born in 1991 in Delhi, India. She received her B.Sc. Honours degree in 2012 and M.Sc. in Chemistry in 2014 from the Institute for Excellence in Higher Education in Bhopal, India. Her master's project at Nirmal University in India focused on biochemistry techniques involving enzyme screening, purification, and characterization. She has 2 years of experience with developing thermoresponsive polymeric hydrogels as a research assistant at Amity University in India. She is currently pursuing her Ph.D. at the University of California, Irvine under the supervision of Dr. Reginald Penner, and her research focuses on the development of virus-based impedimetric biosensors for the rapid detection of cancer biomarkers.

Nicholas P. Drago was born in July 1996 in Palos Heights, IL, and earned a B.S. degree in Chemistry from Elmhurst University in 2018. He is a graduate student studying physical chemistry at the University of California, Irvine. He conducts research in Dr. Reginald Penner's lab, with a focus on polymer-based point-of-care electrochemical biosensing.

Sudipta Majumdar was born in India in 1977. He is a Senior Research Scientist in the Weiss laboratory, focusing on engineering proteins. He completed his Ph.D. under the supervision of Nobel Laureate Robert Huber and Tad A. Holak at the MPI for Biochemistry in Munich, Germany, and did his postdoctoral work at UC Irvine. His research interests include phage display and characterization of proteins. He has worked at Sanofi (India) as a Scientist (R&D). He has received the Crystal Structure Award for his contributions in solving structures of proteins. Recently he was awarded the outstanding reviewer accolade by Elsevier.

Emily C. Sanders received her B.S. in Biochemistry at Western Washington University in 2016. She is currently a Ph.D. candidate in Chemistry at the University of California, Irvine under the supervision of Prof. Gregory Weiss. Her research interests are interdisciplinary in nature and broadly revolve around the interface of molecular biology and polymer chemistry.

Gregory A. Weiss was born in New York City in 1970. He earned a B.S. degree from the University of California, Berkeley, where he conducted research with Paul Bartlett, and a Ph.D. from Harvard University, working with Stuart L. Schreiber. Awarded an NIH Kirschstein NRSA, he pursued postdoctoral studies at Genentech with Jim Wells. In 2000 he joined the faculty at the University of California, Irvine, where his laboratory focuses on combinatorial biology, continuous flow biosynthesis, and bioelectronics. Tenured in 2006, he is currently a full Professor and Vice Chair of the Department of Chemistry.

Reginald M. Penner was born in 1960 in Canada. He is an electrochemist who received a B.A. degree in Chemistry and Biology from Gustavus Adolphus College and a Ph.D. with Charles Martin at Texas A&M University. He studied with Nate Lewis as a postdoctoral fellow at Stanford and Caltech and joined the Department of Chemistry at University of California, Irvine in 1990. His research group investigates electrochemical methods for preparing nanomaterials and studies applications for these nanomaterials in sensors, energy storage, and photonic devices. Presently, he is Chancellor's Professor and Associate Dean for Research and Innovation in the School of Physical Sciences at UCI.

ACKNOWLEDGMENTS

R.M.P. gratefully acknowledges the financial support of this work by the National Science Foundation through contract CBET-1803314. R.M.P. and G.A.W. both gratefully acknowledge support from the National Cancer Institute of the NIH (1R33CA206955-01), PhageTech Inc. (PHAGE-203015), and the Chao Family Comprehensive Cancer Center, UC Irvine. FE-SEM data were acquired using the instrumentation of the LEXI and IMRI (http://www.imri.uci.edu/) facilities at UCI. We thank the healthy urine donors who consented to have their urine used in this study through UCI Clinical Protocol IRB HS# 2014-1758.

REFERENCES

(1) Yang, L. M. C.; Tam, P. Y.; Murray, B. J.; McIntire, T. M.; Overstreet, C. M.; Weiss, G. A.; Penner, R. M. Virus Electrodes for Universal Biodetection. *Anal. Chem.* **2006**, *78*, 3265−3270.

https://dx.doi.org/10.1021/acs.accounts.0c00474
Acc. Chem. Res. XXXX, XXX, XXX−XXX

(2) Donavan, K. C.; Arter, J. A.; Weiss, G. A.; Penner, R. M. Virus-Poly(3,4-Ethylenedioxythiophene) Biocomposite Films. *Langmuir* **2012**, *28*, 12581−12587.
(3) Bhasin, A.; Ogata, A. F.; Briggs, J. S.; Tam, P. Y.; Tan, M. X.; Weiss, G. A.; Penner, R. M. The Virus Bioresistor: Wiring Virus Particles for the Direct, Label-Free Detection of Target Proteins. *Nano Lett.* **2018**, *18*, 3623−3629.
(4) Bhasin, A.; Sanders, E. C.; Ziegler, J. M.; Briggs, J. S.; Drago, N. P.; Attar, A. M.; Santos, A. M.; True, M. Y.; Ogata, A. F.; Yoon, D. V.; et al. Virus Bioresistor (VBR) for Detection of Bladder Cancer Marker DJ-1 in Urine at 10 PM in One Minute. *Anal. Chem.* **2020**, *92*, 6654−6666.
(5) Smith, G. P.; Petrenko, V. A. Phage Display. *Chem. Rev.* **1997**, *97*, 391−410.
(6) Smith, G. P. Phage Display: Simple Evolution in a Petri Dish (Nobel Lecture). *Angew. Chem., Int. Ed.* **2019**, *58*, 14428−14437.
(7) Winter, G.; Milstein, C. Man-Made Antibodies. *Nature* **1991**, *349*, 293−299.
(8) Marks, J. D.; Hoogenboom, H. R.; Bonnert, T. P.; McCafferty, J.; Griffiths, A. D.; Winter, G. By-Passing Immunization: Human Antibodies from V-Gene Libraries Displayed on Phage. *J. Mol. Biol.* **1991**, *222*, 581−597.
(9) Li, Z.; Chen, G. Y. Current Conjugation Methods for Immunosensors. *Nanomaterials* **2018**, *8*, 278−283.
(10) Petrenko, V. A.; Vodyanoy, V. J. Phage Display for Detection of Biological Threat Agents. *J. Microbiol. Methods* **2003**, *53*, 253−262.
(11) Petrenko, V. A. Landscape Phage as a Molecular Recognition Interface for Detection Devices. *Microelectron. J.* **2008**, *39*, 202−207.
(12) Nanduri, V.; Sorokulova, I. B.; Samoylov, A. M.; Simonian, A. L.; Petrenko, V. A.; Vodyanoy, V. Phage as a Molecular Recognition Element in Biosensors Immobilized by Physical Adsorption. *Biosens. Bioelectron.* **2007**, *22*, 986−992.
(13) Yang, L.-M. C.; Diaz, J. E.; McIntire, T. M.; Weiss, G. A.; Penner, R. M. Covalent Virus Layer for Mass-Based Biosensing. *Anal. Chem.* **2008**, *80*, 933−943.
(14) Yang, L.-M. C.; Diaz, J. E.; McIntire, T. M.; Weiss, G. A.; Penner, R. M. Direct Electrical Transduction of Antibody Binding to a Covalent Virus Layer Using Electrochemical Impedance. *Anal. Chem.* **2008**, *80*, 5695−5705.
(15) Zhang, S.; Huang, F.; Liu, B.; Ding, J.; Xu, X.; Kong, J. A Sensitive Impedance Immunosensor Based on Functionalized Gold Nanoparticle-Protein Composite Films for Probing Apolipoprotein A-I. *Talanta* **2007**, *71*, 874−881.
(16) Yan, F.; Sadik, O. A. Enzyme-Modulated Cleavage of DsDNA for Supramolecular Design of Biosensors. *Anal. Chem.* **2001**, *73*, 5272−5280.
(17) Yan, F.; Sadik, O. A. Enzyme-Modulated Cleavage of DsDNA for Studying Interfacial Biomolecular Interactions. *J. Am. Chem. Soc.* **2001**, *123*, 11335−11340.
(18) Ruan, C.; Yang, L.; Li, Y. Immunobiosensor Chips for Detection of Escherichia Coli O157:H7 Using Electrochemical Impedance Spectroscopy. *Anal. Chem.* **2002**, *74*, 4814−4820.
(19) Liu, J.; Tian, S.; Nielsen, P. E.; Knoll, W. In Situ Hybridization of PNA/DNA Studied Label-Free by Electrochemical Impedance Spectroscopy. *Chem. Commun.* **2005**, 2969−2971.
(20) Yang, L.; Li, Y.; Erf, G. F. Interdigitated Array Microelectrode-Based Electrochemical Impedance Immunosensor for Detection of *Escherichia coli* O157:H7. *Anal. Chem.* **2004**, *76*, 1107−1113.
(21) Taggart, D. K.; Yang, Y.; Kung, S.-C.; McIntire, T. M.; Penner, R. M. Enhanced Thermoelectric Metrics in Ultra-Long Electrodeposited PEDOT Nanowires. *Nano Lett.* **2011**, *11*, 125−131.
(22) Xiang, C.; Kung, S.-C.; Taggart, D. K.; Yang, F.; Thompson, M. A.; Güell, A. G.; Yang, Y.; Penner, R. M. Lithographically Patterned Nanowire Electrodeposition: A Method for Patterning Electrically Continuous Metal Nanowires on Dielectrics. *ACS Nano* **2008**, *2*, 1939−1949.
(23) Xiang, C.; Yang, Y.; Penner, R. M. Cheating the Diffraction Limit: Electrodeposited Nanowires Patterned by Photolithography. *Chem. Commun.* **2009**, 859−873.
(24) Lamboy, J. A.; Arter, J. A.; Knopp, K. A.; Der, D.; Overstreet, C. M.; Palermo, E. F.; Urakami, H.; Yu, T.-B.; Tezgel, O.; Tew, G. N.; et al. Phage Wrapping with Cationic Polymers Eliminates Nonspecific Binding between M13 Phage and High p I Target Proteins. *J. Am. Chem. Soc.* **2009**, *131*, 16454−16460.
(25) Arter, J. A.; Taggart, D. K.; McIntire, T. M.; Penner, R. M.; Weiss, G. A. Virus-PEDOT Nanowires for Biosensing. *Nano Lett.* **2010**, *10*, 4858−4862.
(26) Arter, J. A.; Diaz, J. E.; Donavan, K. C.; Yuan, T.; Penner, R. M.; Weiss, G. A. Virus−Polymer Hybrid Nanowires Tailored to Detect Prostate-Specific Membrane Antigen. *Anal. Chem.* **2012**, *84*, 2776−2783.
(27) Menke, E. J.; Thompson, M. A.; Xiang, C.; Yang, L. C.; Penner, R. M. Lithographically Patterned Nanowire Electrodeposition. *Nat. Mater.* **2006**, *5*, 914−919.
(28) Chang, S. S. Overview of Prostate-Specific Membrane Antigen. *Rev. Urol.* **2004**, *6*, S13−S18.
(29) O'Keefe, D. S.; Bacich, D. J.; Heston, W. D. W. Comparative Analysis of Prostate-Specific Membrane Antigen (PSMA) versus a Prostate-Specific Membrane Antigen-like Gene. *Prostate* **2004**, *58*, 200−210.
(30) Diaz, J. E.; Yang, L.-M. C.; Lamboy, J. A.; Penner, R. M.; Weiss, G. A. Synthesis of a Virus Electrode for Measurement of Prostate Specific Membrane Antigen. *Methods Mol. Biol.* **2009**, *504*, 255−274.
(31) Mohan, K.; Donavan, K. C.; Arter, J. A.; Penner, R. M.; Weiss, G. A. Sub-Nanomolar Detection of Prostate-Specific Membrane Antigen in Synthetic Urine by Synergistic, Dual-Ligand Phage. *J. Am. Chem. Soc.* **2013**, *135*, 7761−7767.
(32) Donavan, K. C.; Arter, J. A.; Pilolli, R.; Cioffi, N.; Weiss, G. A.; Penner, R. M. Virus-Poly(3,4-Ethylenedioxythiophene) Composite Films for Impedance-Based Biosensing. *Anal. Chem.* **2011**, *83*, 2420−2424.
(33) Mohan, K.; Penner, R. M.; Weiss, G. A. Biosensing with Virus Electrode Hybrids. *Curr. Protoc. Chem. Biol.* **2015**, *7*, 53−72.
(34) Ogata, A. F.; Edgar, J. M.; Majumdar, S.; Briggs, J. S.; Patterson, S. V.; Tan, M. X.; Kudlacek, S. T.; Schneider, C. A.; Weiss, G. A.; Penner, R. M. Virus-Enabled Biosensor for Human Serum Albumin. *Anal. Chem.* **2017**, *89*, 1373−1381.
(35) Tan, W. S.; Tan, W. P.; Tan, M.-Y.; Khetrapal, P.; Dong, L.; DeWinter, P.; Feber, A.; Kelly, J. D. Novel Urinary Biomarkers for the Detection of Bladder Cancer: A Systematic Review. *Cancer Treat. Rev.* **2018**, *69*, 39−52.
(36) Kumar, P.; Nandi, S.; Tan, T. Z.; Ler, S. G.; Chia, K. S.; Lim, W.-Y.; Bütow, Z.; Vordos, D.; De laTaille, A.; Al-Haddawi, M.; et al. Highly Sensitive and Specific Novel Biomarkers for the Diagnosis of Transitional Bladder Carcinoma. *Oncotarget* **2015**, *6*, 13539−13549.
(37) Rivnay, J.; Inal, S.; Salleo, A.; Owens, R. M.; Berggren, M.; Malliaras, G. G. Organic Electrochemical Transistors. *Nat. Rev. Mater.* **2018**, *3*, 17086.
(38) Wang, N.; Yang, A.; Fu, Y.; Li, Y.; Yan, F. Functionalized Organic Thin Film Transistors for Biosensing. *Acc. Chem. Res.* **2019**, *52*, 277−287.
(39) Lin, P.; Yan, F.; Chan, H. L. W. Ion-Sensitive Properties of Organic Electrochemical Transistors. *ACS Appl. Mater. Interfaces* **2010**, *2*, 1637−1641.
(40) Li, H.; Shi, W.; Song, J.; Jang, H.-J.; Dailey, J.; Yu, J.; Katz, H. E. Chemical and Biomolecule Sensing with Organic Field-Effect Transistors. *Chem. Rev.* **2019**, *119*, 3−35.
(41) Gao, N.; Zhou, W.; Jiang, X.; Hong, G.; Fu, T.-M.; Lieber, C. M. General Strategy for Biodetection in High Ionic Strength Solutions Using Transistor-Based Nanoelectronic Sensors. *Nano Lett.* **2015**, *15*, 2143−2148.

https://dx.doi.org/10.1021/acs.accounts.0c00474
Acc. Chem. Res. XXXX, XXX, XXX−XXX